

Pseudoheterodyne near-field imaging at kHz repetition rates via quadrature-assisted discrete demodulation

Cite as: Appl. Phys. Lett. **120**, 131601 (2022); <https://doi.org/10.1063/5.0087187>

Submitted: 02 February 2022 • Accepted: 19 March 2022 • Published Online: 31 March 2022

 Samuel Palato,  Philipp Schwendke, Nicolai B. Grosse, et al.

COLLECTIONS

Paper published as part of the special topic on [Optical Nanoprobe Spectroscopy and Imaging](#)



View Online



Export Citation




CrossMark

ARTICLES YOU MAY BE INTERESTED IN


[Long-wave infrared super-resolution wide-field microscopy using sum-frequency generation](#)
Applied Physics Letters **120**, 131102 (2022); <https://doi.org/10.1063/5.0081817>

[A perspective on ultralong silicon nanowires for flexible sensors](#)
Applied Physics Letters **120**, 130501 (2022); <https://doi.org/10.1063/5.0085119>

[Infrared photodetector based on 2D monoclinic gold phosphide nanosheets yielded from one-step chemical vapor transport deposition](#)
Applied Physics Letters **120**, 131104 (2022); <https://doi.org/10.1063/5.0086166>



HIDEN
ANALYTICAL



40
YEARS
1982 - 2022


Instruments for Advanced Science

- Knowledge,
- Experience,
- Expertise

Click to view our product catalogue


Contact Hiden Analytical for further details:
www.HidenAnalytical.com
info@hideninc.com

Gas Analysis




- ▶ dynamic measurement of reaction gas streams
- ▶ catalysis and thermal analysis
- ▶ molecular beam studies
- ▶ dissolved species probes
- ▶ fermentation, environmental and ecological studies

Surface Science




- ▶ UHVTPD
- ▶ SIMS
- ▶ end point detection in ion beam etch
- ▶ elemental imaging - surface mapping

Plasma Diagnostics



- ▶ plasma source characterization
- ▶ etch and deposition process reaction kinetic studies
- ▶ analysis of neutral and radical species

Vacuum Analysis



- ▶ partial pressure measurement and control of process gases
- ▶ reactive sputter process control
- ▶ vacuum diagnostics
- ▶ vacuum coating process monitoring

Pseudoheterodyne near-field imaging at kHz repetition rates via quadrature-assisted discrete demodulation

Cite as: Appl. Phys. Lett. **120**, 131601 (2022); doi: [10.1063/5.0087187](https://doi.org/10.1063/5.0087187)

Submitted: 2 February 2022 · Accepted: 19 March 2022 ·

Published Online: 31 March 2022



View Online



Export Citation



CrossMark

Samuel Palato,^{1,2,a)}  Philipp Schwendke,^{1,2}  Nicolai B. Grosse,³ and Julia Stähler^{1,2} 

AFFILIATIONS

¹Abteilung Physikalische Chemie, Fritz-Haber-Institut der Max-Planck-Gesellschaft, Berlin, Germany

²Institut für Chemie, Humboldt-Universität zu Berlin, Berlin, Germany

³Elektroniklabor, Fritz-Haber-Institut der Max-Planck-Gesellschaft, Berlin, Germany

Note: This paper is part of the APL Special Collection on Optical Nanoprobe Spectroscopy and Imaging.

^{a)} Author to whom correspondence should be addressed: samuel.palato@hu-berlin.de

ABSTRACT

Scattering-type scanning near-field optical microscopy enables the measurement of optical constants of a surface beyond the diffraction limit. Its compatibility with pulsed sources is hampered by the requirement of a high-repetition rate imposed by lock-in detection. We describe a sampling method, called quadrature-assisted discrete (quad) demodulation, which circumvents this constraint. Quad demodulation operates by measuring the optical signal and the modulation phases for each individual light pulse. This method retrieves the near-field signal in the pseudoheterodyne mode, as proven by retraction curves and near-field images. Measurement of the near-field using a pulsed femtosecond amplifier and quad demodulation is in agreement with results obtained using a CW laser and the standard lock-in detection method.

© 2022 Author(s). All article content, except where otherwise noted, is licensed under a Creative Commons Attribution (CC BY) license (<http://creativecommons.org/licenses/by/4.0/>). <https://doi.org/10.1063/5.0087187>

Scattering-type scanning near-field optical microscopy (s-SNOM) exploits the near-field (NF) enhancement close to the apex of a conductive AFM nanotip to probe the optical properties of a surface with nanometer spatial resolution.^{1–3} In combination with femtosecond pulsed lasers, it is possible to resolve processes with ~ 20 nm and < 50 fs resolutions. Time-resolved SNOM has enabled unprecedented observation of spatiotemporal dynamics, such as resolution and control of exciton–polariton propagation in WSe₂ waveguides,^{4,5} and the dynamics of the formation of a charge-depletion layer in InAs nanowires.⁶

In s-SNOM, the NF signal is extracted from the total backscattered light via the high-order demodulation technique.^{1,2,7} In the standard implementation, the measurement employs lock-in detection, which imposes constraints on the repetition rate of pulsed lasers. For high-harmonic demodulation, the AFM is operated in the tapping mode with frequency Ω , dictated by the mechanical resonance of the cantilever. The NF signal is detected at higher harmonics $n\Omega$ for sufficiently large n . Imaging in the visible regime typically requires $n > 3$. Artifact-free imaging further requires the use of a local oscillator (LO) to carry out a form of interferometric detection such as pseudoheterodyne

detection (pshet). In the pshet mode, the phase of the LO is modulated sinusoidally at frequency M . The NF signal can be recovered from the amplitudes of the sidebands⁸ at frequencies $n\Omega + mM$. For imaging in the visible range using standard cantilevers, this electronic signal is located around 1.1 MHz. The high frequency of detection imposes a constraint on the repetition rate of the pulsed laser: measurement by lock-in detection requires a repetition rate of at least twice the detection frequency.⁹ This constraint forces compromises between the AFM parameters and laser amplifier. In most cases, it precludes the use of kHz class laser amplifiers.^{9,10}

Here, we demonstrate pshet SNOM imaging with a 200 kHz femtosecond laser amplifier, a commercial optical unit for pshet SNOM and a custom detection module. Wang *et al.* demonstrated that it is possible to recover the self-homodyne NF signal even in the case of an irregular repetition rate by measuring the signal as a function of the phase of the tapping modulation.¹⁰ Phase-domain sampling methods enable measurement of the near-field interaction even with stochastic measurement times such as for single photon detection.^{11–13} We improve on the phase-domain sampling approach of Wang *et al.* by measuring the modulation phases using an in-phase component

X and a quadrature component Y and by extending the method to pshet SNOM. Employing an auxiliary quadrature channel enables the efficient calculation of the modulation phases at arbitrary points in time. Sampling is, therefore, performed at a rate given by the repetition rate of the laser. The measurement of the optical signal as functions of the phases of both modulations is readily Fourier-transformed to yield a matrix of coefficients $u_{n,m}$, equivalent to the sideband amplitudes of lock-in detection. This method, quadrature-assisted discrete (quad) demodulation, enables the real time processing of the NF signal. The validity of the method is confirmed by retraction curves and imaging on a reference grating.

Quad demodulation uses the pshet optical detection module of a commercial s-SNOM (neaSNOM, NeaSpec).⁸ Figure 1(a) shows a scheme of the optical components. The input laser beam is supplied by a Nb:KGW regenerative amplifier with a repetition rate of $f_{\text{rep}} = 200$ kHz (Pharos, Light Conversion) and an optical parametric amplifier (OPA, Orpheus-3H, Light Conversion). A flip mirror in the beam path enables switching between the pulsed source and a CW HeNe laser (HNL150L, Thorlabs). To enable comparison of results obtained with the two sources, our OPA is tuned to a central wavelength of $\lambda_0 = 633$ nm. The FWHM spectral bandwidth is $\Delta\lambda = 30$ nm. The power and polarization of the input beam are controlled using a variable neutral density (ND) filter as well as a $\lambda/2$ waveplate and polarizer assembly (not shown). A spatial filter and 3:1 beam expander (not shown) ensure a large, high-quality, and constant transverse mode. The power at the input of the interferometer is 3–4 mW when using the HeNe laser and 300 μ W when using the OPA. The interferometer splits the input beam equally into the signal and reference arms. In the signal arm, a parabolic mirror focuses the beam onto the apex of a PtIr-coated AFM tip (Arrow NCPT, Nanoworld). The AFM is operated in the tapping mode with a tip oscillation frequency Ω between 240 and 380 kHz and a contact tapping amplitude $A \approx 80$ nm. The backscattered light, which contains contributions from the NF signal as well as from the diffraction-limited background, is collected using the same parabolic

mirror. The reference arm is equipped with a piezo-driven end mirror, which enables the modulation of the path length of the reference arm at frequency $M \approx 300$ Hz and modulation depth $\gamma = 2.63$ rad. An ND filter inserted in the reference arm controls the intensity of the LO. The two arms recombine at the beam splitter and are sent toward a Si photoreceiver with adjustable gain (OE-300-SI-10, Femto Messtechnik). By virtue of its compatibility with standard optical elements, it is possible to switch between quad demodulation and lock-in detection by switching the laser sources and detection modules.

In pshet SNOM, the NF signal is retrieved using the two modulations: tip tapping and phase of the LO. We now summarize this detection scheme; a complete description is available in the literature.^{2,8,9} The intensity at the detector is $S = |E_{\text{BG}} + E_{\text{NF}} + E_{\text{LO}}|^2$, where BG denotes the diffraction limited background, NF is the desired near-field signal, and LO is the local oscillator. By modulating both the NF and the LO, it is possible to isolate the interference term $E_{\text{NF}}E_{\text{LO}}^*$. The motion of the tip quickly varies the height h of the tip above the sample and, therefore, the magnitude of the NF signal. The nonlinear dependency of the NF signal in h gives rise to components at higher harmonics of the tapping frequency $n\Omega$. Measurement of the higher harmonics enables the separation of the BG and NF contributions.¹ When done in the absence of a local oscillator, this signal is known as the self-homodyne (shd) signal. Pshet improves on this method by employing a phase modulated LO. The motion of the end mirror modulates the optical phase of the LO ψ_{LO} sinusoidally with amplitude γ and frequency M . In the strong phase modulation regime ($\gamma \gg 0.2$), this modulation gives rise to multiple sidebands in the frequency domain with frequency shifts mM . The amplitude of a given sideband is $|u_{n,m}| \propto J_m(\gamma)$, where $J_m(\gamma)$ is the Bessel function of the first kind. Furthermore, sidebands with odd and even m can be combined to gain phase information. By selecting $\gamma = 2.63$, it has been shown^{2,8} that the NF signal of order n can be calculated as $s_n \propto u_{n,2} + iu_{n,1}$. The phase $\varphi_n = \arg(s_n)$ is related to the phase of the NF signal. By applying two modulations and combining the resulting sidebands,

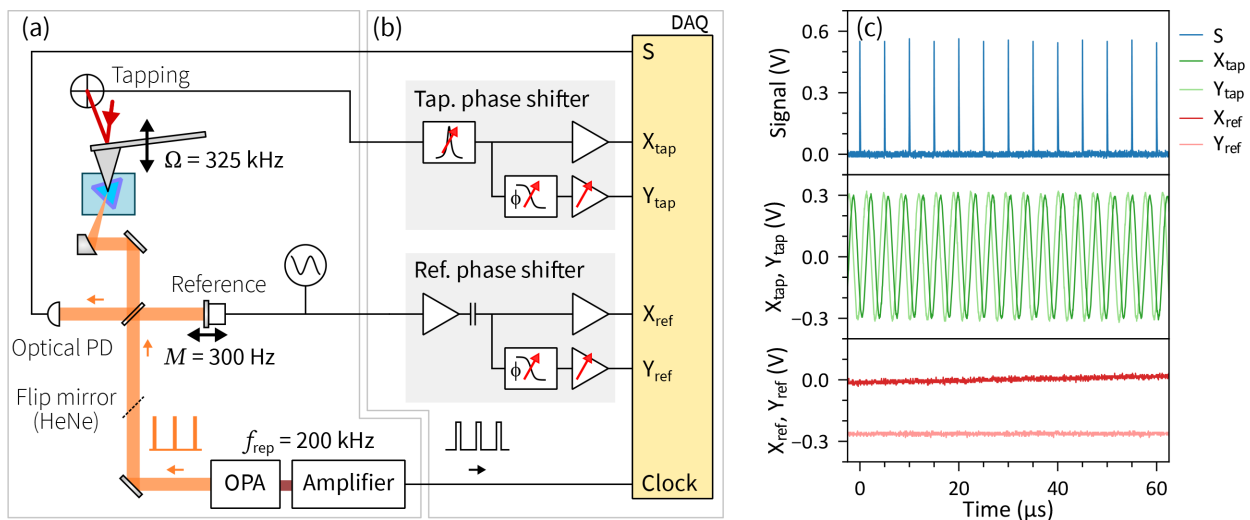


FIG. 1. Scheme of the apparatus and raw signals. (a) Diagram of the optical components for SNOM in the pshet mode. (b) Diagram of the detection module for quad demodulation. See the text for a detailed description. (c) Raw signals. A single measurement is performed on each channel for every pulse. The individual optical pulses are resolved. The use of two components for each modulation enables the measurement of the phases at arbitrary time points.

pshet improves signal quality, enables artifact-free imaging, and yields phase information.^{8,9} Despite the increased spectral bandwidth of femtosecond pulses, they can still be used in the pshet mode when the spectral bandwidth is smaller than 10% of the central frequency,⁹ as is the case for our OPA. In the standard implementation, the sidebands are measured via lock-in detection. We employ the standard lock-in technique and the CW HeNe laser to provide reference measurements and compare them with the results of quad demodulation.

In quad demodulation, the NF is obtained by measuring the optical signal as a function of the phases of the modulations. In the phase domain, the modulations are

$$h = A[1 - \cos(\theta_{\text{tap}} - \theta_C)], \quad (1)$$

$$\psi_{\text{LO}} = \gamma \cos(\theta_{\text{ref}} - \theta_0) + \psi_R, \quad (2)$$

where θ_{tap} is the phase of the tapping modulation, θ_C is the phase at contact, θ_{ref} is the phase of the reference arm modulation, θ_0 is an offset for θ_{ref} , and ψ_R is an offset for the optical phase. The other symbols have been introduced above. The electronic detection module for quad demodulation enables the measurement of the relationship $S(\theta_{\text{tap}}, \theta_{\text{ref}})$ from which the pshet signal can be retrieved.

The detection electronics for quad demodulation enables measurement of the NF signal with kHz pulsed sources. Figure 1(b) shows a scheme of the electronics device. The device consists of two home-built analogue phase shifter units and a multifunction data acquisition card (DAQ, USB-6356, National Instruments). The phase shifter units enable the efficient measurement of the modulation phases. These units take the modulation signal as their input and generate an in-phase component X and a quadrature component Y . An independent phase shifter is used for each modulation. For the tapping modulation, the phase shifter unit uses the deflection signal from the AFM. A tunable active bandpass filter at the input stage removes residual noise from the deflection photodiode electronics. The bandpass filter generates the in-phase component X_{tap} . The second channel employs an adjustable all-pass filter and an output buffer with adjustable gain to generate a quadrature component Y_{tap} . The phase shifter for reference arm modulation uses a similar design with a few modifications. The input signal is obtained directly from the waveform generator driving the pshet piezo. The input is AC-coupled and then separated into two signals X_{ref} and Y_{ref} as before. The phase shifters are calibrated to achieve equal amplitudes and a $\pi/2$ phase shift between the X and Y components. Following this calibration, the phases can be straightforwardly calculated at arbitrary time points as $\theta = \arctan(Y/X)$. As a result of this design, the measured phase is robust against variations of the modulation amplitudes or offsets, which occur during normal operation of the device.

The signals are sampled by the DAQ once for each pulse. Figure 1(c) shows, as an example, the signals available at the DAQ. DAQ cards synchronized with the laser pulses are versatile and performant acquisition systems for optical experiments.¹⁴ A trigger derived from the optical pulse train ensures synchronization and is used as a sampling clock for the DAQ. The optical signal consists of the train of pulses from the interferometer. The sampling clock is adjusted to sample the maximum of this signal. The modulation signals are sampled simultaneously with the optical channel using independent analog to digital converters. Tapping modulation is visible as a pair of sinusoids with a short period in Fig. 1(c). The reference

modulation signals have a low frequency of ~ 300 Hz and only vary slowly on this timescale. Using the synchronized DAQ and the phase shifter units, the optical signal S and the modulation phases θ_{ref} and θ_{tap} are measured for each individual pulse.

In the following, the NF signal is obtained from the measurements of individual pulses using Fourier analysis—in a process analogous to standard lock-in detection. Figure 2 illustrates the processing steps. The measurement process samples the signal as a function of the two modulation phases $S(\theta_{\text{tap}}, \theta_{\text{ref}})$, sampled at arbitrary locations. The Fourier transform (FT) on non-uniform grids is a common problem in fields such as astronomy.¹⁵ In order to perform the demodulation, we extend the phase-binning approach of Wang *et al.*¹⁰ to two dimensions. The data are first regularized by grouping the points into

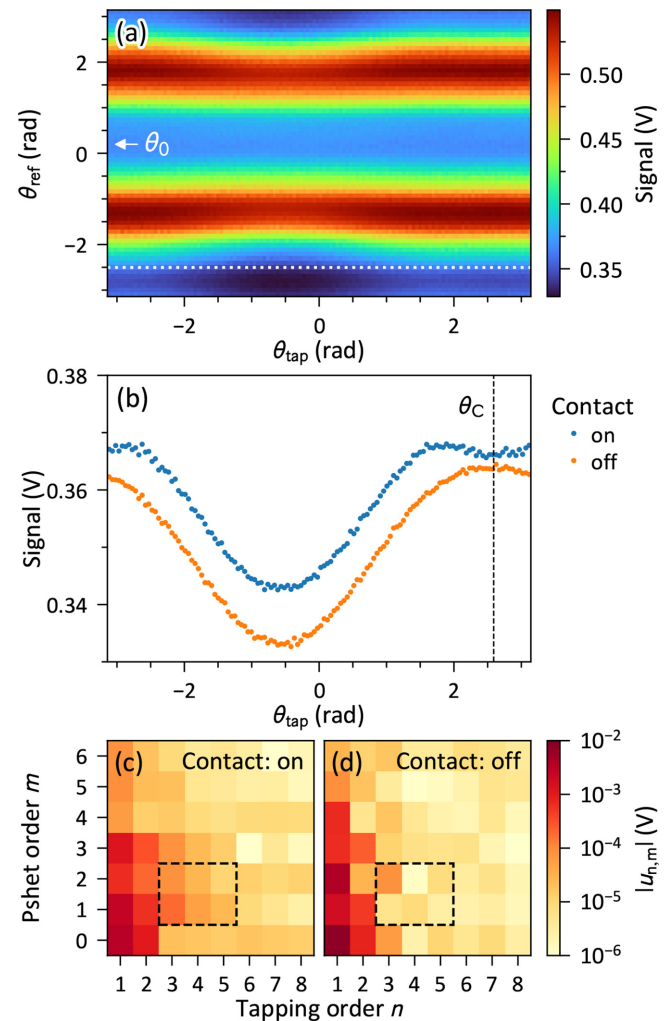


FIG. 2. Quad demodulation of the pshet signal. (a) Signal as a function of the modulation phases after regularization. (b) Cut at a fixed value of θ_{ref} , indicated by the dotted line in panel (a). The point of contact is visible as a dip around $\theta_C = 2.6$ rad. The curve for off-contact has been shifted and scaled to facilitate comparison. (c) Demodulated pshet signal $u_{n,m}$ as a function of tapping order n and pshet order m in contact. The dashed box indicates the location of the NF signal. (d) Same as in (c), off-contact.

2D bins and performing the average for each bin. The per-bin average is a split-apply-combine algorithm and can, therefore, be performed easily and efficiently using common data analysis packages such as pandas. An example of data after regularization is shown in Fig. 2(a) using 128 bins along θ_{tap} and 64 bins along θ_{ref} . The largest pattern present in the data is due to reference arm modulation, which gives rise to horizontal stripes. The pattern is symmetric around θ_0 , which can be determined by the FT along θ_{ref} and taking the phase of the first harmonic ($m = 1$). The exact shape of the pattern is dictated by γ and ψ_R .

The impact of tip tapping can be seen by selecting the data at a single value of θ_{ref} , yielding a cut equivalent to a homodyne measurement. The resulting data are shown in Fig. 2(b), both on and off contact. The exact location of the cut is shown as a dotted line in Fig. 2(a). In contact, the cut has the shape of a sinusoid with an extra contribution around the maximum, which is absent when the tip is off contact. This observation enables the determination of the phase at contact θ_C . As θ_{tap} is derived from the output of the AFM deflection detector, the method already corrects for drifts of the mechanical phase that occur during scanning. Therefore, θ_C does not depend on the position of the sample relative to the cantilever nor on tip-sample interaction. The value of θ_C is a property of the instrument related to the different detection delay in the optical and modulation electronics. We determine this value from the FT of the data along θ_{tap} and taking the phase of the first harmonic ($n = 1$). In our experience, this value is highly stable. The specific behavior of the optical signal at θ_C varies depending on the relative phase of the NF and background electric fields, which is difficult to control experimentally.^{8,10}

In order to perform phase demodulation, the data in the phase-phase domain [Fig. 2(a)] are Fourier transformed along both dimensions. This transformation directly yields a matrix of the coefficients $u_{n,m}$, equivalent to the sideband amplitudes using standard lock-in detection. Figure 2(c) shows an example of this matrix. For optimal noise rejection, knowledge of θ_C and θ_0 are used to phase the FT. The regularized data $S(\theta_{\text{tap}}, \theta_{\text{ref}})$ [Fig. 2(a)] are first Fourier transformed along θ_{tap} using θ_C as a phase offset to yield $S(n, \theta_{\text{ref}})$. As per Eq. (1), the signal is contained in the real part of $S(n, \theta_{\text{ref}})$ for all orders n . A second FT along θ_{ref} results in the matrix $u_{n,m}$ with non-negative n and m . Using θ_0 as a phase offset again enables noise rejection by keeping the real part only [see Eq. (2)]. As previously described,^{2,8} the complex NF signal is obtained from this matrix as $s_n = u_{n,2} + iu_{n,1}$. The NF signal is, therefore, located in the region $n > 2$ and $0 < m < 3$. This signal disappears when off contact, as shown in Fig. 2(d).

In summary, quad demodulation of the raw dataset containing the measurements of individual pulses is performed in three steps: (i) calculation of the phases, (ii) binning, and (iii) phased FT. The phases are calculated geometrically, binning is carried-out by a split-apply-combine operation, and the Fourier transform uses standard FFT. The entire analysis is, therefore, remarkably quick. The signal analysis for 75 000 points, acquired in 375 ms, is performed in 30 ms on a standard personal computer, using code available in standard libraries (numpy, pandas). Quad demodulation satisfies the conditions of real-time processing and allows continuous acquisition, processing, and display. This capability enables quad demodulation to be used directly during initial alignment as well as for monitoring during the acquisition of an image.

The measurement of the NF signal is confirmed by its disappearance when the tip loses contact. Figure 3 shows retraction curves: the

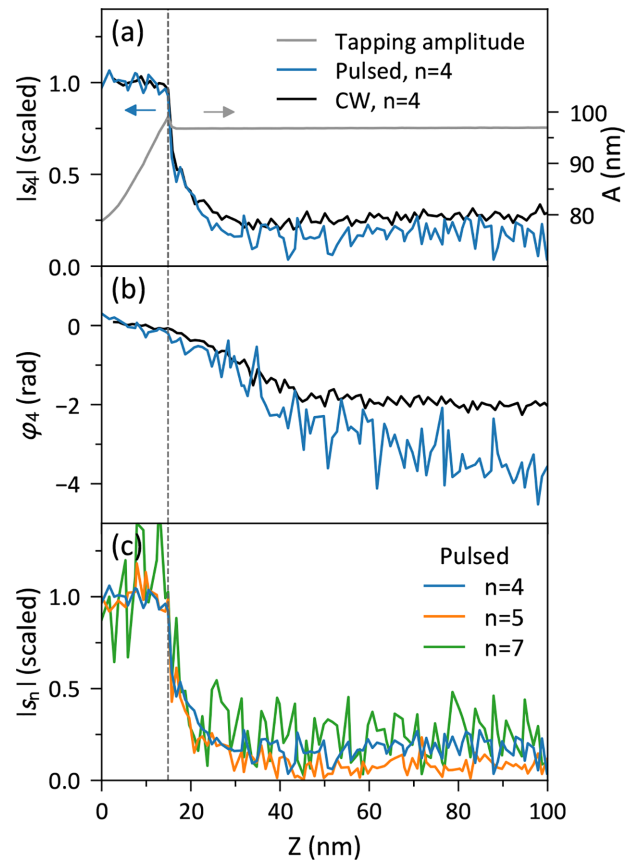


FIG. 3. Retraction curves confirm the NF signal. (a) Comparison of the NF signal amplitudes obtained with the pulsed laser and quad demodulation vs a standard CW HeNe laser and lock-in detection. The AFM tapping amplitude is also shown. (b) Comparison of the optical phases of the NF signal. The phase shift relative to the average in contact is shown. (c) The measurement of isolated femtosecond pulses enables the acquisition of high tapping orders n via quad demodulation and the pulsed laser. The curves in panels (a) and (c) have been divided by their average value in contact to enable comparison.

optical signal as the distance Z between the cantilever and sample is increased. The measurements were performed in ambient conditions on the Si substrate of a calibration grating (TGQ1, Tips-Nano). The vertical dashed line indicates the point where the contact is lost, as determined from the AFM tapping amplitude A [gray curve in panel (a)]. Figures 3(a) and 3(b) show the amplitude and phase of the NF signal obtained using the pulsed laser and quad demodulation (blue) to results obtained using a CW HeNe laser and the standard lock-in demodulation (black). The amplitudes have been divided by their average value in contact to facilitate comparison but to preserve contrast. The phases have been shifted by their average value in contact as the absolute phase is arbitrary. Figure 3(a) shows the NF signal vanishes very quickly upon losing contact, thereby demonstrating that the NF signal is uncontaminated by background contributions. The optical phase ϕ_n , displayed in Fig. 3(b), shows similar trends for both measurements with a well-defined optical phase when in contact. The measurements were performed independently, on different days, with

intervening tip changes and optical realignment. As the measurements are obtained with different light sources and different measurement modules, we consider the agreement is excellent, and it confirms the equivalence between both methods. The behavior of the retraction curve demonstrates the capacity of quad demodulation to measure the NF signal and its equivalence to lock-in detection.

By exploiting the stroboscopic effect, quad demodulation enables the practical measurement of the NF signal for higher orders than possible with standard methods. Figure 3(c) shows retraction curves confirming the measurement of the NF signal up to $n=7$, equivalent to a frequency of ~ 2.2 MHz, via quad demodulation. All curves show a similar behavior indicative of the NF signal. The measurement of demodulation orders for $n > 4$ via standard methods requires a bandwidth larger than 1.25 MHz or sampling rates larger than 2.5 MHz. Quad demodulation isolates these signals despite the detection electronics being limited to 1 MHz and a low sampling rate of 200 kHz. The capacity of quad to detect high frequency signals is due to the very short duration of the optical pulses. Each pulse, therefore, samples the NF interaction at a very well-defined position of the tip. This measurement method is analogous to flash photography, where the time resolution is dictated by the duration of the flash instead of camera exposure time.¹⁶ The largest order accessible to quad demodulation is not dictated by the detector response but instead by signal to noise considerations. Similar approaches that correlate an optical signal to the modulation phase or vertical distance with high resolution enable the observation of subtle spectral changes of the NF signal with tip-sample distance.¹⁷ Due to its ability to resolve high demodulation orders, quad demodulation is ideally suited for NF tomography.^{6,18}

We now demonstrate NF imaging by quad sampling. Figure 4 shows images acquired on the reference grating TGQ1. This grating

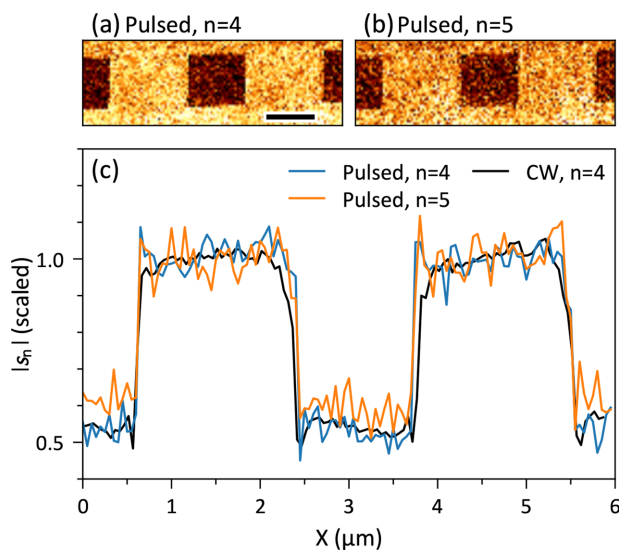


FIG. 4. Near-field imaging using quad demodulation and the pulsed femtosecond laser. (a) Pshet near-field image acquired using the pulsed laser and quad demodulation for order $n=4$. Scale bar has a length of $1 \mu\text{m}$. (b) Same as panel (a) for $n=5$. (c) Horizontal profiles taken through the images in panels (a) and (b), compared to the results obtained using a HeNe laser and lock-in detection (see the text).

consists of squares of SiO_2 on a Si substrate with a period of $3 \mu\text{m}$ and a height of ~ 20 nm. SiO_2 is a dielectric and has a low NF signal compared to the Si base. Panels (a) and (b) of Fig. 4 show images acquired using quad demodulation for orders $n=4$ and 5. The images confirm the capability of quad demodulation to perform NF imaging. Figure 4(c) shows horizontal profiles acquired using quad demodulation and with the standard lock-in technique. For comparison, all profiles have been scaled to the NF signal value on Si but not shifted in order to preserve contrast information. For $n=4$, the results obtained with quad demodulation are in quantitative agreement with the results obtained with the standard method, despite the use of different laser sources and acquisition modules. These NF images confirm the capacity of quad sampling to produce measurements equivalent to the standard lock-in method.

In conclusion, we described a method to perform near-field imaging in the pshet mode with a kHz class laser amplifier. Quadrature-assisted discrete demodulation retrieves the near-field signal from the measurements of the backscattered light for individual pulses. To assist in signal retrieval, the state of each modulation is recorded using both an in-phase and a quadrature channel. The efficient demodulation algorithm enables real time demodulation of the near-field signal in the pshet mode. The retrieved signal is in agreement with results obtained using the standard lock-in detection method. By exploiting the stroboscopic effect, quad demodulation circumvents the bandwidth limits of traditional methods and enables the measurement of the near-field signal for high demodulation orders. This development extends the range of light sources compatible with SNOM and unlocks access to the broad toolkit of nonlinear optics available to kHz amplifiers such as femtosecond pump-probe measurements, wavelength tunable sources, and white-light continuum generation. Quad demodulation may also be useful to realize experiments that were previously impossible due to a mismatch between the modulation frequency and the optical repetition rate.

This work was funded by the Deutsche Forschungsgemeinschaft (DFG, German Research Foundation)—Project ID: 182087777—SFB 951. S.P. acknowledges funding from the Alexander von Humboldt foundation. S.P., P.S., and J.S. thank Sarah King and Jun Nishida for stimulating discussions. We also thank the team at the ELAB, and in particular, Georg Hammer for the extensive wiring.

AUTHOR DECLARATIONS

Conflict of Interest

The authors have no conflicts to disclose.

DATA AVAILABILITY

The data that support the findings of this study are available from the corresponding author upon reasonable request.

REFERENCES

- ¹M. B. Raschke and C. Lienau, *Appl. Phys. Lett.* **83**, 5089 (2003).
- ²J. M. Atkin, S. Berweger, A. C. Jones, and M. B. Raschke, *Adv. Phys.* **61**, 745 (2012).
- ³D. N. Basov, M. M. Fogler, and F. J. García De Abajo, *Science* **354**, aag1992 (2016).
- ⁴A. J. Sternbach, S. Latini, S. Chae, H. Hübener, U. De Giovannini, Y. Shao, L. Xiong, Z. Sun, N. Shi, P. Kissin, G. X. Ni, D. Rhodes, B. Kim, N. Yu, A. J.

- Millis, M. M. Fogler, P. J. Schuck, M. Lipson, X. Y. Zhu, J. Hone, R. D. Averitt, A. Rubio, and D. N. Basov, *Nat. Commun.* **11**, 3567 (2020).
- ⁵M. Mrejen, L. Yadgarov, A. Levanon, and H. Suchowski, *Sci. Adv.* **5**, eaat9618 (2019).
- ⁶M. Eisele, T. L. Cocker, M. A. Huber, M. Plankl, L. Viti, D. Ercolani, L. Sorba, M. S. Vitiello, and R. Huber, *Nat. Photonics* **8**, 841 (2014).
- ⁷R. Hillenbrand and F. Keilmann, *Phys. Rev. Lett.* **85**, 3029 (2000).
- ⁸N. Ocelic, A. Huber, and R. Hillenbrand, *Appl. Phys. Lett.* **89**, 101124 (2006).
- ⁹A. J. Sternbach, J. Hinton, T. Slusar, A. S. McLeod, M. K. Liu, A. Frenzel, M. Wagner, R. Iraheta, F. Keilmann, A. Leitenstorfer, M. Fogler, H.-T. Kim, R. D. Averitt, and D. N. Basov, *Opt. Express* **25**, 28589 (2017).
- ¹⁰H. Wang, L. Wang, and X. G. Xu, *Nat. Commun.* **7**, 12744 (2016).
- ¹¹B. D. Mangum, E. Shafran, C. Mu, and J. M. Gerton, *Nano Lett.* **9**, 3440 (2009).
- ¹²J. Tisler, T. Oeckinghaus, R. J. Stöhr, R. Kolesov, R. Reuter, F. Reinhard, and J. Wrachtrup, *Nano Lett.* **13**, 3152 (2013).
- ¹³E. Shafran, B. D. Mangum, and J. M. Gerton, *Nano Lett.* **10**, 4049 (2010).
- ¹⁴C. A. Werley, S. M. Teo, and K. A. Nelson, *Rev. Sci. Instrum.* **82**, 123108 (2011).
- ¹⁵J. T. VanderPlas, *Astrophys. J. Suppl. Ser.* **236**, 16 (2018).
- ¹⁶H. E. Edgerton, *Electronic Flash, Strobe* (McGraw-Hill Inc., 1970), p. 384.
- ¹⁷H. Wang, L. Wang, D. S. Jakob, and X. G. Xu, *Nat. Commun.* **9**, 2005 (2018).
- ¹⁸A. A. Govyadinov, S. Mastel, F. Golmar, A. Chuvilin, P. S. Carney, and R. Hillenbrand, *ACS Nano* **8**, 6911 (2014).